Relativistic Positron Creation Using Ultraintense Short Pulse Lasers

Hui Chen,[1] Scott C. Wilks,[1] James D. Bonlie,[1] Edison P. Liang,[2] Jason Myatt,[3] Dwight F. Price,[1] David D. Meyerhofer,[3] and Peter Beiersdorfer[1]

[1]*Lawrence Livermore National Laboratory, Livermore, California 94550, USA*
[2]*Rice University, Houston, Texas 77005, USA*
[3]*University of Rochester, Rochester, New York 14623, USA*

(Received 5 September 2008; published 11 March 2009)

We measure up to 2×10^{10} positrons per steradian ejected out the back of ~mm thick gold targets when illuminated with short (~1 ps) ultraintense ($\sim 1 \times 10^{20}$ W/cm^2) laser pulses. Positrons are produced predominately by the Bethe-Heitler process and have an effective temperature of 2–4 MeV, with the distribution peaking at 4–7 MeV. The angular distribution of the positrons is anisotropic. Modeling based on the measurements indicate the positron density to be $\sim 10^{16}$ positrons/cm^3, the highest ever created in the laboratory.

DOI: 10.1103/PhysRevLett.102.105001 PACS numbers: 52.38.Ph, 52.59.−f

The ability to rapidly create large numbers of MeV positrons in the laboratory opens the door to new avenues of antimatter research, including an understanding of the physics underlying various astrophysical phenomena such as black holes and gamma ray bursts [1,2], pair plasma physics [3,4], positronium production, and positronium Bose-Einstein condensates [5–7]. The use of short, ultraintense, lasers represents a promising new approach to achieve this. Since first theorized in 1973 [8], the use of ultraintense lasers to generate positrons has been studied in great detail through theory and modeling [9–15]. It has been predicted that for thick high-Z targets, positron generation through the Bethe-Heitler (BH) process [16] dominates over the Trident process [16,12,13]. For thin targets (less than 30 microns for solid gold), the reverse is expected [9]. In the BH process, laser-produced hot electrons make high-energy bremsstrahlung photons that produce electron-positron pairs by interacting with the nuclei, while in the Trident process, the hot electrons produce pairs directly interacting with the nuclei. Although estimates vary, approximately 10^{10} to 10^{11} positrons/kJ of laser energy are predicted to be created, assuming various laser target conditions [13–15]. Experimentally, the ability of intense short laser pulses to create positrons in laser-solid interaction was first demonstrated on the Nova peta-watt laser by Cowan *et al.* [17] and later on a tabletop laser by Gahn *et al.* [18], where small numbers of positrons were measured.

In this Letter, up to 2×10^{10} positrons/sr with positron kinetic energy up to 20 MeV were observed by irradiating ~millimeter thick gold targets with short-pulse lasers. Positron temperatures were measured for the first time, and were found to be about half that of hot electron temperature. A strong anisotropy in the angular positron emission was observed, with the number ejected near the normal to the rear of the target being more than 10 times the number more obliquely observed from the front of the target on a given shot. The positron density inside the target is estimated to be about 10^{16} positrons/cm^3, making this the densest collection of positrons produced in the laboratory [19]. These conclusions result from the best statistics and energy resolution positron spectra ever obtained using short-pulse lasers. The data are consistent with the BH process in which positrons were produced by MeV photons interacting with gold nuclei.

The experiment was carried out at the Titan laser at the Jupiter laser facility [20] at Lawrence Livermore National Laboratory. For the experiments described here, the pulse-length of the laser (1054 nm, *s*-polarized) was varied between 0.7 to 10 ps, and the laser energy was between 120 to 250 J. The pre-pulse to main-pulse intensity contrast is less than 10^{-5}. Focused with an $f/3$ off-axis parabola, the full-width at half-maximum of the focal spot was about 8 microns and contains about 60% of laser energy. The experimental setup is shown in Fig. 1. The short pulse was incident to the targets at an 18-degree angle. Two absolutely calibrated electron-positron spectrometers [21] observed the hot electrons and the positrons from the targets with energy coverage from 0.1–100 MeV and a resolution $E/\delta E$ of 10–100, much improved from the previous positron spectrometer from which a hint of positron signal was observed [22]. The energy coverage and resolution are higher than previously achieved in positron energy mea-

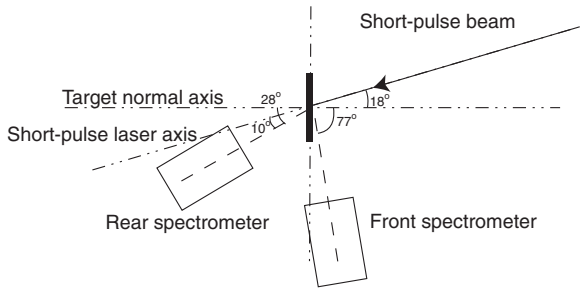

FIG. 1. Illustration of the experimental set up. The location of two spectrometers relative to the lasers and target is marked.

surement [17,18], where positrons were measured at one [18] or several energy points [17]. The absolute calibration was made using electrons [23]. Because there is little difference (~2–3%) in positron and electron stopping in the detector materials [24], the electron calibration is applicable to the positrons. The solid angle for the rear spectrometer is 8.2×10^{-5} steradian and 4.5×10^{-5} steradian for the front spectrometer. The targets were disks of solid gold ($Z = 79$), tantalum ($Z = 73$), tin ($Z = 50$), copper ($Z = 29$), and aluminum ($Z = 13$) with 6.38 mm diameter and thicknesses between 0.1 to 3.1 mm.

The peak short-pulse laser intensity ranged from 3×10^{19} to 2×10^{20} W/cm^2 primarily due to variations in the pulse length. The effective hot electron temperatures for electrons with energies between 5 MeV and the maximum (~60 MeV) were 3.2 to 9.4 MeV, about 2 to 4 times higher than that predicted by the ponderomotive scaling [25]. This is attributed to self-modulated laser wakefield acceleration of electrons [26] in the large preformed plasma that substantially enhances the temperature. The scale length of the preformed underdense plasma was estimated to be between 5 to 15 microns. The difference from ponderomotive scaling is more pronounced when the pulse length is longer. The number of hot electrons above 2 MeV (which are relevant to the creation of positrons) was 2.5×10^{11}/sr to 1.4×10^{12}/sr.

Positron signals from Au and Ta targets were observed once the thickness exceeded 250 microns. Figure 2 shows the raw data image for a 1 mm Au target and the line out through the signal and background. The background was mainly caused by high-energy photons passing through the housing of the spectrometer into the detector. Those photons were both directly from the target and from secondary radiation around the target chamber. The background evenly illuminates the detector beyond the slit, and therefore it is easily subtracted from the signal, which came only from the collimator and slit of the spectrometer. The signal was verified to be from positrons using methods such as differentiating particles using mass stopping by adding plastic foils, and shooting lower-Z targets, such as Al, Cu, and Sn for the same laser conditions as for shooting Au targets. While the hot electron production for those lower-Z targets was similar to that from Au, there was no positron signal above the background. The absence of signal was consistent with the Z^4 scaling of the BH positron yield that would result in more than an order of magnitude fewer positrons in these lower-Z targets [13]. For thinner (0.1 to 0.25 mm) Au targets, positrons were not observed above the background. This is because fewer pairs would be produced from thinner targets [13] due to the reduced interaction range between photons and electrons with Au nuclei. Thinner targets have more high-energy photon yield [27] contributing to a higher background and therefore a higher positron detection threshold.

The yield of positrons was determined by scaling positrons to the number of hot electrons detected. Figure 3 shows the electron spectrum from the rear spectrometer and the positron spectra from both the front and rear spectrometers for a 126 J, 2 ps shot, the same shot as in Fig. 2. The electron spectrum from the front spectrometer is similar to that of the rear spectrometer and is not in-

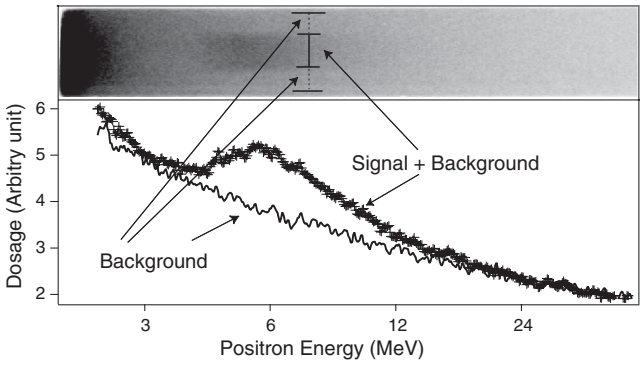

FIG. 2. Raw positron data image and line outs. This shot had 2 ps and 126 J. The laser intensity was about 6×10^{19} W/cm^2. The target thickness was 1 mm.

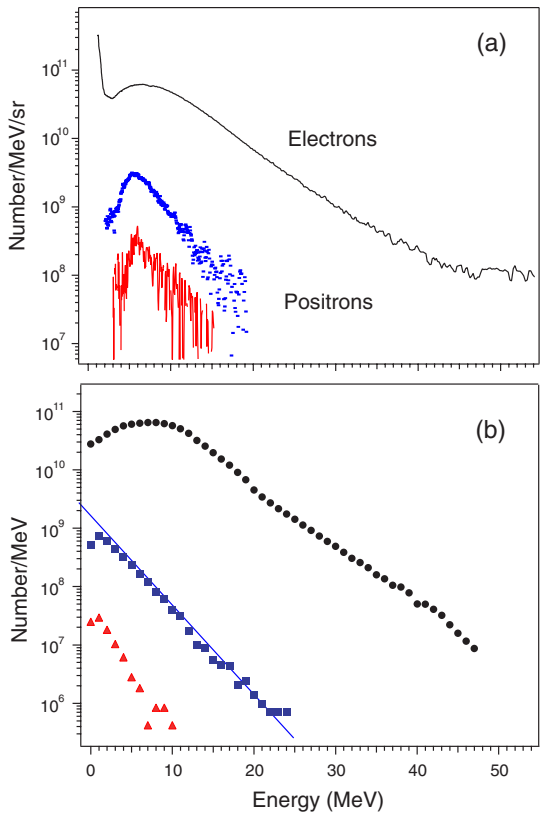

FIG. 3 (color online). Energy spectra of electrons and positrons from experiments (a) and EGS modeling (b). On both (a) and (b), the electron spectrum is at the top and the two positron spectra are at the bottom. The positron spectrum from the back of the target has the higher number of counts of the two. The solid line in (b) is the slope from the analytic formula.

cluded. The detection limit is about 1×10^8/MeV/sr for the rear and about 2×10^7/MeV/sr for the front spectrometer. The higher energy section (5–45 MeV) of the electron spectrum is more relevant to positron creation, and it had a temperature (the slope of the energy spectrum) of 4.8 ± 0.4 MeV and an electron number of about 7×10^{11}/sr. The positron numbers are about 1.6×10^{10}/sr from the rear and 2×10^9/sr from the front spectrometer. The peaks of both positron spectra are at about 6 MeV, and the effective positron temperature is 2.8 ± 0.3 MeV. This first experimental positron temperature measurement enabled the electron and positron temperatures to be compared: the measured positron temperature was found to be approximately half that of the effective electron temperature. This may be explained as follows: an electron (via a photon) in the original electron spectra is, in effect, splitting its energy into the newly created positron and electron. Therefore, one would expect the positron to be half as energetic as the source electron.

A strong anisotropy in the angular positron emission was observed from the rear and front of the target as shown in Fig. 3(a), with the number ejected near the normal to the rear of the target being more than 10 times the number more obliquely observed from the front of the target on a given shot. This is the first observation of an anisotropic distribution of the laser-generated positrons.

While the inferred hot electron numbers for the Nova peta-watt experiment [17] were similar to that measured in this experiment, more than 2 orders of magnitude more positrons were observed in the rear of the target from the present experiment than that on Nova peta-watt experiment, where the positrons were measured at the rear of the target, 30 degrees from the laser axis [17]. This may be due to the preformed plasma conditions, and target thickness (~1 mm versus 0.125 mm on Nova PW), and possibly a suboptimal observation angle used in Nova.

Calculations using the measured hot electron temperature show that the BH process dominates the positron production process in thick targets. The ratio of positrons generated by the BH versus Trident processes is $N_{\mathrm{BH}}/N_{\mathrm{Trident}} \sim 400$ for 1 mm thick Au (compared to about 4 for a 0.1 mm Au target.) The positron temperature can be estimated from a simple formula $dN_{e+}/dE_{e+} = \int_E f(E)\sigma_{\mathrm{BH}}(E, E_{e+})dE$, where $f(E)$ is the bremsstrahlung photon energy distribution, and σ_{BH} is the positron creation differential cross section [16]. Approximating the bremsstrahlung temperature to be that of the measured hot electrons, an effective temperature for the positrons of about half that of the electrons is obtained, as shown in Fig. 3(b). This is consistent with the experimental data [Fig. 3(a)]. The positron spectrum obtained from the above calculation is for all positrons generated inside the target. To model the emergent positron spectrum measured by the spectrometer, one has to fold in the positron transport inside the target. This was accomplished by a Monte Carlo code EGSNRC [28]. This code includes only BH pair production and is well suited for our thick target cases. In addition to calculating the positron generation, it self-consistently treats the attenuation effects of the electrons, photons, and positrons as they propagate through a cold solid target. The measured hot electron temperature shown in Fig. 3(b) is used as the starting distribution of hot electrons. The positron spectra outside the target were modeled at the same angular positions relative to the target as in the experiment. The simulated positron spectra agree not only with the positron temperature (slope of the spectrum) seen in the experiment, but also with the relative positron number. We note that the peak of positrons from the simulation is at about 2 MeV (as in a previous prediction [13]), rather than at the measured ~6 MeV. This discrepancy may be due to the fact that neither the analytic formula nor EGS simulations include plasma effects. For example, a sheath electric field is expected to accelerate the positrions leaving the target, similar to the target normal sheath acceleration field (typically of order of several MeV) for protons [29]. This is supported by the fact that protons with energies of 1–4 MeV were observed at the rear of the target for the shot shown in Fig. 3 and the same sheath field that accelerates the protons would certainly influence the front and rear positron spectra.

The yield of positrons increases as a function of hot electron temperature for a given target thickness, as predicted theoretically [13,15]. The yield of positrons also increases as a function of target thickness, as shown in Fig. 4. Theoretically, the increase of positron yield with target thickness has been shown for thinner targets by Nakashima and Takabe [13]. For a thick target (2 mm lead), Gahn *et al.* [30] calculated that for an electron kinetic energy above 5–15 MeV, the positron yield is between 5×10^{-3} and 4×10^{-2}, comparable to our measured yield of about 2×10^{-2}. Figure 4 shows the results from the analytical model and simulation using EGS for these experimental conditions. In the analytic model, the yield was estimated using the BH pair creation process combined with positron and electron attenuation inside the

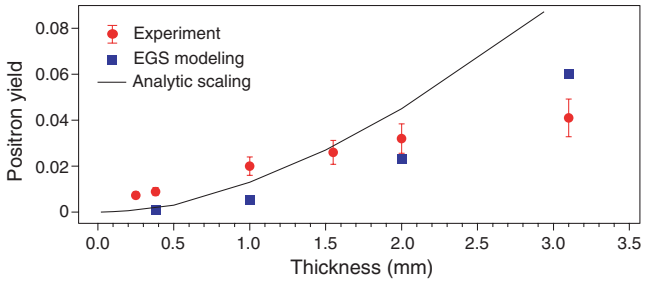

FIG. 4 (color online). Positron yield per hot electron as a function of Au target thickness. The short-pulse duration was 0.7 ps for all data points. The laser intensities were from $1.5–1.8 \times 10^{20}$ W/cm^2, hot electron temperature from 5.5–7 MeV.

target, indicating that the positron yield per hot electron detected increases as target thickness, until the target thickness is greater than about 5–6 mm. Although there is a general qualitative agreement between theory or modeling and experiments, both the analytic model and the EGS simulation underestimate the positron yield for thickness less than 1 mm. This difference may again be due to differences in angular distributions of positrons versus electrons and complex plasma effects, such as electron or positron transport and the electromagnetic field, lacking in the theory and EGS modeling.

The rear spectrometer data corresponds to 2×10^{10} observed positrons/sr for about 120 J laser energy for 1 mm target. From the EGS simulations, at least a factor of 10 more positrons is expected to be trapped inside the target. Given the bremsstrahlung photon and target interaction volume determined from the simulation to be approximately 2×10^{-5} cm^3, the positron density in the target is estimated to be about 1×10^{16} positrons/cm^3, which is the highest MeV positron density ever created in the laboratory, albeit in the presence of gold atoms at solid density. If all of the positrons are created in the order of ~ps, then the rate of positron production is of the order of 2×10^{22}/s/sr. In the future, as higher energy (100's of Joules), high repetition rate (>10 Hz) short-pulse laser sources become available, the average positron production rate could approach 10^9/s/sr, which is comparable to existing positron sources [19]. Since the number of positrons scales with energy, 10 times this rate is expected from a kJ class short-pulse laser like OMEGA EP laser [31] and even higher numbers with lasers such as NIF-ARC [32].

These results potentially enable many important applications of intense positron sources. For example, the understanding of many astrophysical phenomena, from pulsar winds to gamma ray bursts [2], hinges on the understanding of pair-dominated and hybrid pair-electron-ion plasmas [15]. Another important application of intense positron sources is the formation of high-density positronium (Ps) gas. Because of its short lifetime (0.14 msec for ortho-Ps, 0.1 ns for para-Ps), current Ps densities achievable in the laboratory [19] are strongly limited by the positron flux available to create Ps ($<10^9$ $e+$/s). Since our laser-produced positron flux is orders of magnitude higher, a completely new regime is now, in principle, accessible to Ps physics. Finally, to achieve a Bose-Einstein condensate (BEC) at liquid helium temperature, the Ps density needed is about 4×10^{17} cm^{-3} [7,33], which is only a factor of ~40 higher than the positron density reported in this Letter. Even though the conversion efficiency of MeV positrons to slow positrons and then to Ps would be much less than unity, given the observed favorable scaling of positron yield with increasing target thickness and laser energy, it may be possible to create a BEC of Ps with future higher energy lasers.

Work performed under the auspices of U.S. DOE by LLNL under Contract No. DE-AC52-07NA27344, LDRD-08-LW-058, and ILSA. Work by the U of R supported by U.S. DOE No. DE-FC5208NA28302, U of R, and the NY ERDA. Work performed by Rice U. under NSF No. AST-0406882.We gratefully acknowledge support from JLF staff, M. Eckart, W. Craig, W. Goldstein, and D. Correll, and discussions with R. Heeter, M. Schneider, and R. Shepherd.

[1] J. Wardle *et al.*, Nature (London) **395**, 457 (1998).
[2] P. Meszaros, Annu. Rev. Astron. Astrophys. **40**, 137 (2002).
[3] H. A. Weldon, Phys. Rev. Lett. **66**, 293 (1991).
[4] E. G. Blackman and G. B. Field, Phys. Rev. Lett. **71**, 3481 (1993).
[5] P. M. Platzman and A. P. Mills, Jr., Phys. Rev. B **49**, 454 (1994).
[6] A. P. Mills, Jr., Nucl. Instrum. Methods Phys. Res., Sect. B **192**, 107 (2002).
[7] E. P. Liang and C. D. Dermer, Opt. Commun. **65**, 419 (1988).
[8] J. W. Shearer *et al.*, Phys. Rev. A **8**, 1582 (1973).
[9] E. P. Liang, S. C. Wilks, and M. Tabak, Phys. Rev. Lett. **81**, 4887 (1998).
[10] B. Shen and J. Meyer-ter-Vehn, Phys. Rev. E **65**, 016405 (2001).
[11] P. L. Shkolnikov *et al.*, Appl. Phys. Lett. **71**, 3471 (1997).
[12] D. A. Gryaznykh, Y. Z. Kandiev, and V. A. Lykov, JETP Lett. **67**, 257 (1998).
[13] K. Nakashima and H. Takabe, Phys. Plasmas **9**, 1505 (2002).
[14] V. I. Berezhiani, D. P. Garuchava, and P. K. Shukla, Phys. Lett. A **360**, 624 (2007).
[15] J. Myatt *et al.* (unpublished).
[16] W. Heitler, *The Quantum Theory of Radiation* (Clarendon Press, Oxford, 1954).
[17] T. E. Cowan *et al.*, Laser Part. Beams **17**, 773 (1999).
[18] C. Gahn *et al.*, Appl. Phys. Lett. **77**, 2662 (2000).
[19] C. M. Surko and R. G. Greaves, Phys. Plasmas **11**, 2333 (2004).
[20] http://jlf.llnl.gov.
[21] H. Chen *et al.*, Rev. Sci. Instrum. **79**, 10E533 (2008).
[22] H. Chen *et al.*, Rev. Sci. Instrum. **77**, 10E703 (2006).
[23] H. Chen *et al.*, Rev. Sci. Instrum. **79**, 033301 (2008).
[24] F. Rohrlich and B. C. Carlson, Phys. Rev. **93**, 38 (1954).
[25] S. C. Wilks *et al.*, Phys. Rev. Lett. **69**, 1383 (1992).
[26] J. Krall *et al.*, Phys. Rev. E **48**, 2157 (1993); N. E. Andreev *et al.*, Phys. Scr. **49**, 101 (1994); C. D. Decker and W. B. Mori, Phys. Rev. Lett. **72**, 490 (1994); E. Esarey *et al.*, Phys. Rev. Lett. **72**, 2887 (1994).
[27] S. P. Hatchett *et al.*, Phys. Plasmas **7**, 2076 (2000).
[28] I. Kawrakow and D. W. O. Rogers, National Research Council of Canada Report No. PIRS-701 2006.
[29] S. C. Wilks *et al.*, Phys. Plasmas **8**, 542 (2001).
[30] C. Gahn *et al.*, Phys. Plasmas **9**, 987 (2002).
[31] L. J. Waxer *et al.*, Opt. Photonics News **16**, 30 (2005).
[32] M. H. Key, Phys. Plasmas **14**, 055502 (2007).
[33] D. B. Cassidy and A. P. Mills, Jr., Phys. Status Solidi A **4**, 3419 (2007).